

## Research paper

An impulsive model predictive static programming based station-keeping guidance for quasi-halo orbits<sup>☆</sup>

Srianish Vutukuri\*, Radhakant Padhi

Dept. of Aerospace Eng., Indian Institute of Science, Bangalore, India



## ARTICLE INFO

## Keywords:

Circular restricted three body problem  
 Elliptic four body problem  
 Quasi-halo orbits  
 Station-keeping  
 Model predictive static programming

## ABSTRACT

In this paper, a control effort minimizing optimal station-keeping guidance is designed and implemented to regulate a spacecraft around an  $L_1$  quasi-halo orbit in the Sun–Earth–Moon elliptic four-body problem. The station-keeping guidance is formulated as a finite time, non-linear optimal control problem with hard terminal output constraints and Impulsive Model Predictive Static Programming (I-MPSP) is used to obtain station-keeping maneuvers. The algorithm is iterative, where the guessed station-keeping maneuvers are optimally updated by a simple closed-form equation until an output terminal constraint is satisfied and an optimal cost function is obtained. The technique involves the calculation of sensitivity matrices that is done in a computationally efficient manner owing to their recursive nature. Through extensive simulations, in the presence of disturbance forces and uncertainties, a closed-loop application of I-MPSP guidance results in a trajectory that remains tightly bound to the reference orbit over a long-duration mission.

## 1. Introduction

A spacecraft sent to a Lagrange point is placed in a Lagrange-point orbit (LPO) suitable for its scientific mission. The three collinear Lagrange points and various orbits surrounding them are unstable, and therefore any perturbations and uncertainties affecting the spacecraft may result in its deviation from the reference LPO. If the deviation is left unchecked, the spacecraft will eventually escape the Lagrange point region, which results in the failure of the mission. To avoid this scenario, station-keeping maneuvers are executed periodically in order to keep the spacecraft close to the reference orbit. Hence the station-keeping controller must be effective for a long duration orbital maintenance, and as well as be robust against unknown disturbances and modeling uncertainties.

The design of station-keeping algorithms can be broadly classified according to a continuous or impulsive form of control implementation [1]. A continuous form of station-keeping guidance [2–5] is typically required during low-thrust missions where the necessary velocity change is imparted by firing the engines for a long duration. An impulsive form of station-keeping guidance is preferred during high-thrust mission scenarios where the thruster firing times to impart the required velocity are very short compared to the period of the reference orbit. Impulsive forms of station-keeping control have been the most frequently used techniques for several practical missions and will be examined in this work.

The impulsive form of station-keeping control was first formulated by Lidov et al. [6,7] as a regulation problem. In this method, the dynamics of the spacecraft are linearized around the Lagrange point, and an appropriate station-keeping maneuver is obtained. Ilyin [8] proposed another impulsive strategy to bound the spacecraft around the Lagrange point by stabilizing the coefficient of the unstable eigenvector of the linearized dynamics. Elyasberg and Timokhova [9] proposed an impulsive station-keeping strategy based on the method of osculating parameters.

The use of Floquet theory as a potential strategy for station-keeping around reference LPOs first appeared in the works of Kogan [10], Simó et al. [11] and Gómez et al. [12]. In the Floquet mode approach, the spacecraft is stabilized around the reference LPO by computing a maneuver that eliminates the largest unstable component of motion along the Floquet basis of the linearized reference orbit. Even though these techniques are simple for implementation, the station-keeping maneuvers obtained by linear approximation of the reference trajectory may not be effective for large spacecraft deviations. In addition, there is no quantitative control over the final deviation of the spacecraft from the reference orbit.

The target point approach (TPA) and its variations [13–15], was proposed by Howell et al. [16], in which an impulsive station-keeping maneuver is computed by minimizing a weighted cost function expressed as a function of maneuver cost and deviations from the reference trajectory at specified future times. The deviations from the

<sup>☆</sup> The work was supported by a research grant (Grant No: ISTC-19-0004) from the Space Technology Cell at the Indian Institute of Science, Bangalore, India.

\* Corresponding author.

E-mail addresses: [srianishv@iisc.ac.in](mailto:srianishv@iisc.ac.in) (S. Vutukuri), [padhi@iisc.ac.in](mailto:padhi@iisc.ac.in) (R. Padhi).

reference orbit are estimated using state transition matrices (STMs). As STMs are obtained via linearization around the reference orbit, estimation of future deviations may become unreliable when the spacecraft is far away from the reference orbit or for a longer prediction time. Compared to the Floquet mode approach, quantitative control over future deviations is incorporated as a soft constraint by minimizing the spacecraft deviation as a part of the cost function.

A multiple-impulses optimization (MIO) method was proposed by Ghorbani and Assadian [17] in which by formulating a non-linear programming problem (NLP), the authors compute fuel-efficient trajectories around  $L_1$  and  $L_2$  points of the Earth–Moon system. In the presence of unknown disturbances and uncertainties, the closed-loop implementation of the NLP-based optimization technique becomes computationally intensive.

The existing station-keeping algorithms are primarily based on linear techniques and therefore become ineffective for large spacecraft deviations from the reference orbit. For any halo orbit mission, apart from the station-keeping cost, the position divergence of the spacecraft from the nominal orbit is equally important. It is known that the traditional station-keeping approaches result in a linear position divergence [18–20] during a long-duration mission. Even though non-linear and optimal control based guidance techniques are desirable, they are often computationally intensive. Addressing these issues, in this paper, a computationally efficient, non-linear optimal station-keeping guidance is proposed for regulating a spacecraft around LPOs.

The station-keeping controller is formulated as a finite time, non-linear optimal control problem and the Impulsive Model Predictive Static Programming (I-MPSP) technique [21] is applied to obtain optimal station-keeping maneuvers. The I-MPSP technique developed by Sakode and Padhi [22] solves a finite time, discrete optimal control problem subject to impulse controls and terminal output constraints. It is an emerging technique with its core philosophy based on Model Predictive Static programming [23,24]. The salient features of the I-MPSP based station-keeping controller can be summarized as follows. The final deviation of the spacecraft from the reference orbit is formulated as a finite time, hard, terminal output constraint. The technique results in a minimum control-effort optimal solution. The method involves the computation of sensitivity matrices that are calculated in a recursive manner. In addition to the above advantages, the controller has a simple, closed-form structure.

Typically a station-keeping mission is affected by the accuracy of the dynamical model, type of reference LPO, disturbance forces, and modeling uncertainties. In reality, the non-zero eccentricity of Earth's orbit and the Moon's gravitational influence in the vicinity of the Sun–Earth  $L_1$  point have a significant influence on the spacecraft trajectory. Ignoring these dynamic effects while formulating the station-keeping controller will lead to unrealistic station-keeping costs and large spacecraft deviations. In addition, periodic halo orbits around collinear Lagrange points in circular restricted three-body problem (CR3BP) exist as quasi-periodic halo's in the more accurate dynamical model. In view of these arguments, in this work, the I-MPSP based station-keeping controller is used to tightly regulate a spacecraft around an  $L_1$  quasi-halo orbit in the Sun–Earth–Moon elliptic four-body problem (E4BP).

Another significant force affecting the spacecraft motion near the  $L_1$  region is solar radiation pressure (SRP). In this work, the SRP force acting on the spacecraft in its Sun-pointing configuration is included in the nominal system dynamics. In the spacecraft propagation model, the nominal dynamics of the spacecraft are further subjected to an unknown SRP force resulting from uncertainty in the coefficient of reflectivity. Sensor inaccuracies are also incorporated into the nominal model in the form of errors in orbital insertion and orbit determination. In the presence of various navigational errors, the I-MPSP based station-keeping guidance results in a spacecraft trajectory that remains tightly bound to the reference quasi-halo orbit.

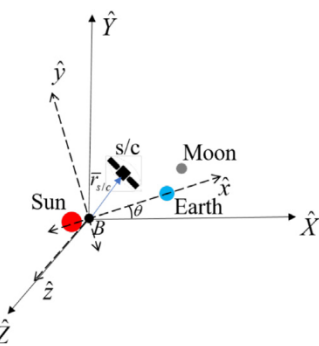


Fig. 1. Illustration of Sun–Earth–Moon E4BP.

Table 1

Keplerian Orbital parameters in J2000.0 reference frame as on January 1st, 2021.

Orbital parameter	Earth	Moon
Mass	$5.97 \times 10^{24}$ kg	$7.35 \times 10^{22}$ kg
Semi-major Axis	$1.49 \times 10^8$ km	$3.86 \times 10^5$ km
Eccentricity	$1.60 \times 10^{-2}$	$3.75 \times 10^{-2}$
Argument of Ascending Node	208.19°	79.62°
Argument of Periapsis	254.38°	136.38°
Inclination	$2.87^\circ \times 10^{-3}$	5.24°
True Anomaly	357.92°	266.55°

## 2. System modeling

### 2.1. Reference frames

The Sun–Earth–Moon elliptic four-body model is shown in Fig. 1. A J2000 inertial reference frame  $I = \{\hat{X}, \hat{Y}, \hat{Z}\}$  is fixed at the Sun–Earth barycenter. The  $\hat{X}$ -axis points towards the mean vernal equinox at Julian year 2000. The  $\hat{Z}$  axis is normal to the ecliptic plane at Julian year 2000, pointing towards celestial north, and the  $\hat{Y}$  axis completes the right-handed triad. The Earth and the Moon are assumed to revolve independently around the Sun and Earth respectively in elliptic orbits with known Keplerian elements [25] as of January 1, 2021 (cf. Table 1). A synodic reference frame  $S = \{\hat{x}, \hat{y}, \hat{z}\}$  is centered at the Sun–Earth barycenter and has the same angular velocity as that of Earth with respect to the inertial frame  $I$ . The  $\hat{x}$  axis points towards Earth. The  $\hat{z}$  axis is perpendicular to Earth's elliptic orbit, along its angular momentum direction. The  $\hat{y}$  axis completes the right-handed triad. In addition, the mass of the spacecraft  $m_{s/c}$  is negligible when compared to the Sun ( $m_s$ ), Earth ( $m_e$ ) and Moon ( $m_m$ ). The  $S$  frame has an angular velocity  $\dot{\theta}\hat{z}$  with respect to the inertial frame  $F_I$ .  $\dot{\theta}$  represents the instantaneous angular rotation rate of Earth around the Sun on its elliptical orbit.

### 2.2. Spacecraft nominal equations of motion

While carrying out solar observation studies, the spacecraft is oriented in a Sun-pointing direction and is actively controlled using reaction wheels. In this attitude configuration, the spacecraft experiences a continuous force in the form of SRP. Assuming the entire SRP force to be an unknown disturbance will lead to increased station-keeping costs and larger spacecraft deviations from the reference orbit. Hence in this work, a known part of the SRP force is included in the spacecraft nominal dynamics and will be referred to as the nominal SRP. Under these assumptions, the equations of motion [17,26] of a spacecraft written in the synodic frame  $S$  subjected to the nominal SRP force are given by

$$\dot{x} = v_x \quad (1)$$

$$\dot{y} = v_y \quad (2)$$

$$\dot{z} = v_z \quad (3)$$

$$\begin{aligned} \dot{v}_x &= 2\dot{\theta}v_y + \dot{\theta}^2x + \ddot{\theta}y - Gm_s \frac{(x - x_s)}{\|\bar{r}_{s-s/c}\|^3} - Gm_e \frac{(x - x_e)}{\|\bar{r}_{e-s/c}\|^3} \\ &\quad + Gm_m \left( -\frac{(1-\mu)(x_m - x_s)}{\|\bar{r}_{s-m}\|^3} - \frac{\mu(x_m - x_e)}{\|\bar{r}_{e-m}\|^3} - \frac{(x - x_m)}{\|\bar{r}_{s/c-m}\|^3} \right) + \bar{a}_{srp}^x \end{aligned} \quad (4)$$

$$\begin{aligned} \dot{v}_y &= -2\dot{\theta}v_x + \dot{\theta}^2y - \ddot{\theta}x - Gm_s \frac{y}{\|\bar{r}_{s-s/c}\|^3} - Gm_e \frac{y}{\|\bar{r}_{e-s/c}\|^3} \\ &\quad + Gm_m \left( -\frac{(1-\mu)y_m}{\|\bar{r}_{s-m}\|^3} - \frac{\mu y_m}{\|\bar{r}_{e-m}\|^3} - \frac{(y - y_m)}{\|\bar{r}_{s/c-m}\|^3} \right) + \bar{a}_{srp}^y \end{aligned} \quad (5)$$

$$\begin{aligned} \dot{v}_z &= -Gm_s \frac{z}{\|\bar{r}_{s-s/c}\|^3} - Gm_m \frac{z}{\|\bar{r}_{e-s/c}\|^3} \\ &\quad + Gm_m \left( -\frac{(1-\mu)z_m}{\|\bar{r}_{s-m}\|^3} - \frac{\mu z_m}{\|\bar{r}_{e-m}\|^3} - \frac{(y - z_m)}{\|\bar{r}_{s/c-m}\|^3} \right) + \bar{a}_{srp}^z \end{aligned} \quad (6)$$

Here  $\mathbf{X} \in \mathbb{R}^6 = [x, y, z, v_x, v_y, v_z]^T$  represents the position and velocity of the spacecraft in synodic frame  $S$ .  $\dot{\theta}$  and  $\ddot{\theta}$  refer to the instantaneous angular velocity and angular acceleration of the Earth in its elliptical orbit around the Sun. The Moon's position in the synodic frame are given by  $x_m, y_m$  and  $z_m$ .  $\mu = \frac{m_e}{m_s + m_e}$  is the mass parameter of the Sun-Earth CR3BP system. Subscripts  $s/c, s, e, m$  stand for spacecraft, Sun, Earth and Moon respectively. The euclidean distance between object  $i$  and object  $j$  is given by  $\|\bar{r}_{i-j}\|$ . The nominal SRP force  $\bar{a}_{srp}$  is obtained using a cannonball model and is given by

$$\bar{a}_{srp} = \frac{S_M \|\bar{r}_{s-e}\|^2 \bar{C}_r A_{srp}}{m_{s/c} \|\bar{r}_{s-s/c}\|^2 c} \hat{r}_{s-s/c} \quad (7)$$

The magnitude of the SRP force is a function of spacecraft area facing the Sun  $A_{srp}$ , nominal coefficient of reflectivity  $\bar{C}_r$ , spacecraft mass  $m_{s/c}$  and distance from the Sun  $\|\bar{r}_{s-s/c}\|$  and acts along the line joining the Sun and the spacecraft.  $S_M$  and  $c$  represent the mean solar flux and the speed of light, respectively. Both the Sun and Earth always lie along the  $\hat{x}$  axis and their instantaneous positions are given by  $x_s = -\mu \|\bar{r}_{s-e}\|$  and  $x_e = (1-\mu) \|\bar{r}_{s-e}\|$ .

### 2.3. Impulsive model for station-keeping control

In this work, as the station-keeping control problem is analyzed for a high thrust mission scenario, the velocity change incurred by the spacecraft during the station-keeping maneuver is achieved in a very short time compared to the reference orbit period. Therefore, it is reasonable to model the maneuver as an instantaneous change in spacecraft velocity:

$$\begin{bmatrix} x^+ \\ y^+ \\ z^+ \\ v_x^+ \\ v_y^+ \\ v_z^+ \end{bmatrix} = \begin{bmatrix} x^- \\ y^- \\ z^- \\ v_x^- + \Delta v_x \\ v_y^- + \Delta v_y \\ v_z^- + \Delta v_z \end{bmatrix} \quad (8)$$

The superscripts – and + indicate the states just before and after the station-keeping maneuver.  $\mathbf{U} \in \mathbb{R}^3 = [\Delta v_x, \Delta v_y, \Delta v_z]^T$  represents the desired velocity change in the  $S$  frame.

### 2.4. Reference quasi-halo orbit

Near periodic, bounded, three-dimensional quasi-halo orbits form a realistic reference trajectory for a spacecraft in the Sun-Earth  $L_1$  region. In this paper, a reference quasi-halo orbit, as shown in Fig. 2,

of roughly five years duration is constructed using a multiple-shooting-based differential corrections strategy [27] from an  $L_1$  halo orbit that has a similar size as that used in the ISEE-3 and the SOHO missions. Nominal dynamics as defined in Section 2.2 are used in the differential corrections process, and hence, the spacecraft's path on the quasi-halo orbit incorporates the effect of the nominal SRP force. The halo orbit that is used to construct the reference trajectory has an out-of-plane amplitude of 120,000 km ( $z$ ) and a time period of approximately 178 days ( $P$ ).  $O$  represents the point of insertion of the spacecraft in the quasi-halo orbit.

### 3. I-MPSP based station-keeping strategy

The nominal spacecraft dynamics, as shown in Sections 2.2 and 2.3, can be concisely represented as

$$\dot{\mathbf{X}} = \mathbf{f}(\mathbf{X}), \text{ at } t \neq t_j \quad (9)$$

$$\mathbf{X}_j^+ = \mathbf{g}(\mathbf{X}_j^-, \mathbf{U}_j), \text{ at } t = t_j \text{ and } j = 1, 2, \dots, n \quad (10)$$

where  $\mathbf{X} \in \mathbb{R}^6$  denotes the states of the spacecraft. Eq. (9) represents the nominal spacecraft dynamics (Eqs. (1)–(6)). Eq. (10) is the instantaneous change in spacecraft states during the station-keeping maneuver as modeled in Eq. (8).  $\mathbf{X}_j^-$  and  $\mathbf{X}_j^+$  represent the states just before and after the  $j$ th maneuver.  $\mathbf{U}_j \in \mathbb{R}^3$  represents the  $j$ th station-keeping maneuver at time  $t_j$ .

Typically, spacecraft output variables of interest, as a function of states, are given as  $\mathbf{Y} = \mathbf{h}(\mathbf{X})$ . In the station-keeping scenario output variables are chosen to be the state vector, i.e.,  $\mathbf{Y} = \mathbf{h}(\mathbf{X}) = \mathbf{X}$ . At any time instant  $t_0$ , the spacecraft lies in the vicinity of the reference trajectory. The states of the spacecraft and corresponding reference trajectory at  $t_0$  are represented by  $\mathbf{X}(t_0) = \mathbf{X}_{N,0}$  and  $\bar{\mathbf{X}}(t_0) = \bar{\mathbf{X}}_{N,0}$ , respectively. An illustration of the station-keeping formulation is shown in Fig. 3. The I-MPSP station-keeping controller must drive the spacecraft along an optimal trajectory that takes it from a current deviated state  $\mathbf{X}_{N,0}$  to a target state on the reference trajectory  $\bar{\mathbf{X}}(t_0 + T) = \mathbf{Y}^* = \mathbf{X}^*$ , in a finite time interval  $T$ . This is carried out by executing  $n$  optimal impulse maneuvers  $\mathbf{U}_j, j = 1, 2, \dots, n$  between the times  $t_0$  and  $t_0 + T$ . In this work, the temporal locations of impulse maneuvers are fixed, i.e., the maneuvers are placed at uniform intervals of time along the trajectory. Each impulse maneuver is placed at a uniform separation  $T/n$  starting at  $t_0$ . This divides the trajectory into  $n$  segments. Each segment of the trajectory is further discretized into  $N$  states using a Runge-Kutta 4th order formulation and a fixed time step  $\frac{T}{n(N-1)}$ . Then the corresponding non-linear discretized dynamics are represented as

$$\mathbf{X}_{k,j} = \mathbf{F}(\mathbf{X}_{k-1,j}), k = 2, 3, \dots, N \quad (11)$$

$$\mathbf{X}_{1,j} = \mathbf{g}(\mathbf{X}_{N,j-1}, \mathbf{U}_j), j = 1, 2, \dots, n \quad (12)$$

$$\mathbf{Y}_{k,j} = \mathbf{h}(\mathbf{X}_{k,j}) \quad (13)$$

$\mathbf{X}_{k,j}$  represents the state at node  $k$  on the  $j$ th segment of the trajectory. Eq. (12) indicates that an impulse maneuver  $\mathbf{U}_j$  modifies only the state  $\mathbf{X}_{N,j-1}$  to  $\mathbf{X}_{1,j}$ .

Starting with a set of guess station-keeping maneuvers and a deviated initial condition  $\mathbf{X}_{N,0}$ , Eqs. (1)–(6) are integrated using a variable-step, variable-order (VSVO) Adams-Basforth-Moulton ODE113 integrator for a time period  $T$  to result in a terminal output  $\mathbf{Y}_{N,n}$  for the spacecraft that will be different from the desired output  $\mathbf{Y}^*$  located on the reference trajectory. The error in the terminal output for the spacecraft is  $\Delta \mathbf{Y}_{N,n}$ . With a good guess for impulse maneuvers  $\mathbf{U}_j, j = 1, 2, \dots, n$ , the terminal output  $\mathbf{Y}_{N,n}$  will be close to  $\mathbf{Y}^*$  and therefore the terminal output error  $\Delta \mathbf{Y}_{N,n} \approx d\mathbf{Y}_{N,n} = \mathbf{Y}_{N,n} - \mathbf{Y}^*$ . Expanding the terminal output  $\mathbf{Y}_{N,n}$  using a Taylor series about the desired terminal output  $\mathbf{Y}^*$ , truncated to first-order terms is written as

$$d\mathbf{Y}_{N,n} = \left[ \frac{\partial \mathbf{Y}}{\partial \mathbf{X}} \right]_{\mathbf{X}_{N,n}^{i-1}} d\mathbf{X}_{N,n}^i \quad (14)$$

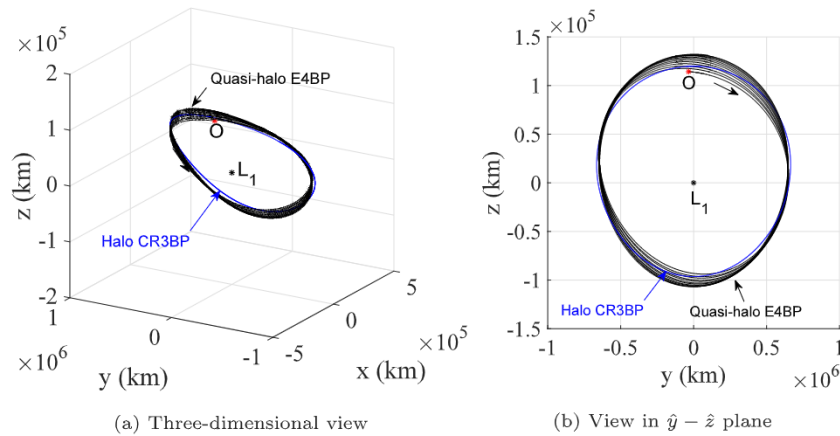


**Fig. 2.** Quasi-halo reference trajectory.

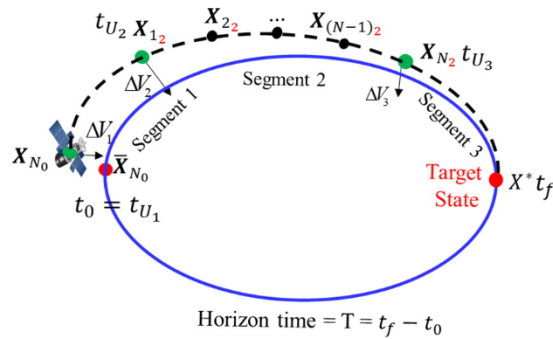


**Fig. 3.** I-MPSP station-keeping formulation.

In Eq. (14),  $dY_{N,n}^i = Y_{N,n}^{i-1} - Y^*$  is the error in the terminal output of the spacecraft during the  $(i)^{th}$  iteration. The term  $dX_{N,n}^i$  is written as a function of error in the previous state  $X_{N-1,n}^i$  at node  $N - 1$  of  $n$ th segment truncated to first-order as

$$d\boldsymbol{X}_{N,n}^i = \left[ \frac{\partial \boldsymbol{F}}{\partial \boldsymbol{X}} \right]_{\boldsymbol{X}_{N-1,n}^{i-1}} d\boldsymbol{X}_{N-1,n}^i \quad (15)$$

Substituting Eq. (15) into Eq. (14) results in

$$dY_{N,n}^i = \left[ \frac{\partial Y}{\partial X} \right]_{X^{i-1}_{N,n}} \left[ \frac{\partial X}{\partial Z} \right]_{X^{i-1}_{N,n}} dZ_{N-1,n}^i \quad (16)$$

The error in the state  $X_{N-1,n}^i$ , i.e.,  $dX_{N-1,n}^i$  is further expressed as a function of error in states at all the previous nodes until the first node of the last segment  $X_1^i$ . Representing the partial derivatives using

$$\left[ \frac{\partial Y}{\partial X} \right]_{X^{i-1}_{N^i}} = C_{N,n}^i, \quad \left[ \frac{\partial F}{\partial X} \right]_{X^{i-1}_j} = A_{k,j}^i \quad (17)$$

and making the necessary substitutions, Eq. (16) can be expanded as

$$dY_{N,n}^i = C_{N,n}^i A_{N-1,n}^i A_{N-2,n}^i \cdots A_{1,n}^i dX_{1,n}^i \quad (18)$$

In the current iteration  $i$ , all the Jacobian matrices in Eq. (18) are evaluated using the states and controls of the  $(i-1)^{th}$  iteration. The first state of the  $n^{th}$  segment  $X_{1,n}^i$  and the last state of the  $(n-1)^{th}$  segment  $X_{N,n-1}^i$  are related by Eq. (12). A Taylor series expansion of Eq. (12) about the desired optimal states and control leads to

$$dX_{1,n}^i = \left[ \frac{\partial g}{\partial X} \right]_{X_{N,n-1}^{i-1}, U_n^{i-1}} dX_{N,n-1}^i + \left[ \frac{\partial g}{\partial U} \right]_{X_{N,n-1}^{i-1}, U_n^{i-1}} dU_n^i \quad (19)$$

The terms  $dX_{1,n}^i$ ,  $dX_{N,n-1}^i$  and  $dU_n^i$  correspond to the errors in states  $X_{1,n}^i$ ,  $X_{N,n-1}^i$  and control  $U_n^i$  with respect to the desired optimal trajectory, respectively. By representing the above partial derivatives using

$$\left[ \frac{\partial g}{\partial X} \right]_{X^{i-1}_{N,j-1}, U^{i-1}_j} = B^i_j, \quad \left[ \frac{\partial g}{\partial U} \right]_{X^{i-1}_{N,j-1}, U^{i-1}_j} = D^i_j \quad (20)$$

Eq. (19) is substituted into Eq. (18) to result in

$$dY_{N,n}^i = C_{N,n}^i A_{N-1,n}^i \cdots A_{1,n}^i B_n^i dX_{N,n-1}^i + C_{N,n}^i A_{N-1,n}^i \cdots A_{1,n}^i D_n^i dU_n^i \quad (21)$$

Eq. (21) is simplified by substituting  $E_n^i = A_{N-1,n}^i A_{N-2,n}^i \cdots A_{1,n}^i$ . The state  $dX_{N,n-1}^i$  is further expressed in terms of errors in states of the segment  $n-1$ . This leads to

$$dY_{N,n}^i = C_{N,n}^i E_n^i B_n^i E_{n-1}^i dX_{1,n-1}^i + C_{N,n}^i E_n^i D_n^i dU_n^i \quad (22)$$

Substituting  $dX_{1:n-1}^i$  in terms of  $dX_{N,n-2}^i$  and  $dU_{n-1}^i$ , (19) is written as

$$dY_{N,n}^i = C_{N,n}^i E_n^i B_n^i E_{n-1}^i B_{n-1}^i dX_{N,n-2}^i + C_{N,n}^i E_n^i B_n^i E_{n-1}^i D_{n-1}^i dU_{n-1}^i \\ + C^i E^i D^i dU^i \quad (23)$$

This process is continued until the terminal output error is finally expressed as a function of errors in impulse maneuvers and initial condition of the spacecraft. The error in the output at final time  $t_f$  is given as

$$d\mathbf{X}^i = Q^i d\mathbf{X}^i + S^i dH^i + S^i dU^i + \dots + S^i dU^i \quad (24)$$

where the matrices in Eq. (34) take the form

$$O^i = C^i - E^i_{\perp} P^i_{\perp} E^i_{\parallel} - E^i_{\parallel} P^i_{\parallel} \quad (25)$$

$$S^i = C^i - E^i P^i E^i - P^i \quad (26)$$

$$S_j = \sum_{N,n} S_n D_n S_{n-1} D_{n-1} \dots S_j D_j \quad (26)$$

The initial condition of the spacecraft is fixed which leads to the term  $d\mathbf{q}^i|_{t=0}$  in Eq. (24) to be zero. Therefore, the error in terminal output is

a function of only errors in impulse maneuvers:

$$dY_{N,n}^i = S_1^i dU_1^i + S_2^i dU_2^i + \cdots + S_{n-1}^i dU_{n-1}^i \quad (28)$$

The matrices  $S_j^i$  are the sensitivity matrices and can be computed in a fast manner owing to their recursive nature. Define matrix  $S_{n,0}^i$  as

$$S_{n,0}^i = C_{N,n}^i E_n \quad (29)$$

Next,  $S_{j,0}^i$  for  $j = (n-1), (n-2), \dots, 1$  are computed recursively as

$$S_{j,0}^i = S_{j+1,0}^i B_{j+1}^i E_j \quad (30)$$

Finally, matrices  $S_j^i$  are obtained as  $S_j^i = S_{j,0}^i D_k^i$  for  $j = n, n-1, \dots, 1$ . For a given error in terminal output  $dY_{N,n}^i$ , the errors in the impulse maneuvers  $dU_j^i, j = 1, 2, \dots, n$  are obtained by solving the linear Eq. (28). When the dimension of the maneuver vector exceeds the dimension of the output constraint (under constrained problem), there is an opportunity to solve Eq. (28) in an optimal manner. The errors in impulse maneuvers are then used to correct the station-keeping maneuvers as  $U_j^i = U_j^{i-1} - dU_j^i, j = 1, 2, \dots, n$ , where  $U_j^i$  and  $U_j^{i-1}$  are the updated and current station-keeping maneuvers. As the magnitude of station-keeping maneuvers corresponds to the amount of propellant consumed, the formulation seeks to achieve the control objective by minimizing a quadratic impulse maneuver function given as

$$J^i = \frac{1}{2} \sum_{j=1}^n (U_j^{i-1} - dU_j^i)^T R_j^i (U_j^{i-1} - dU_j^i) \quad (31)$$

where  $R_j^i$  is a positive semi-definite weight matrix. The optimization variables  $dU_j^i, j = 1, 2, \dots, n$  modify the current station-keeping maneuvers  $U_j^{i-1}$  to  $U_j^i$ . Eq. (31) and (28) form an appropriate static optimization problem. The augmented cost function is written as

$$\bar{J}^i = \frac{1}{2} \sum_{j=1}^n (U_j^{i-1} - dU_j^i)^T R_j^i (U_j^{i-1} - dU_j^i) + (\lambda^i)^T \left( dY_{N,n}^i - \sum_{j=1}^n S_j^i dU_j^i \right) \quad (32)$$

where  $\lambda_j^i$  is the Lagrange multiplier. The necessary conditions of optimality for  $j = 1, 2, 3, \dots, n$  are

$$\frac{d\bar{J}^i}{dU_j^{i-1}} = -R_j^i (U_j^{i-1} - dU_j^i) - (S_j^i)^T \lambda^i = 0 \quad (33)$$

$$\frac{d\bar{J}^i}{d\lambda^i} = dY_{N,n}^i - \sum_{j=1}^n S_j^i dU_j^i = 0 \quad (34)$$

On solving the necessary conditions of optimality, a simple closed-form impulse maneuver update equation  $U_j^i, j = 1, 2, \dots, n$  is obtained as

$$U_j^i = U_j^{i-1} - dU_j^i = -\left(R_j^i\right)^{-1} \left(S_j^i\right)^T (A_\lambda^i)^{-1} \left(dY_{N,n}^i - b_\lambda^i\right) \quad (35)$$

where

$$A_\lambda^i = \left[ \sum_{j=1}^n S_j^i \left(R_j^i\right)^{-1} \left(S_j^i\right)^T \right], b_\lambda^i = \left[ \sum_{j=1}^n S_j^i U_j^{i-1} \right] \quad (36)$$

The new station-keeping maneuvers  $U_j^i, j = 1, 2, \dots, n$  are then used to propagate Eqs. (9) and (10) to result in a new terminal output, that is closer to the target output  $Y^*$ . The station-keeping maneuvers are updated once again by solving the static optimization problem using Eqs. (32)–(35). The sensitivity matrices  $S_j^i, j = 1, 2, \dots, n$  used in the optimization process are re-computed in each iteration using the states and impulses on the last updated trajectory. This process of updating the station-keeping maneuvers is carried out in an iterative manner until the terminal error  $\|dY_{N,n}^i\|_\infty$  and the difference in cost function between consecutive iterations  $|J^i - J^{i-1}|$  is less than a tolerance value.

#### 4. Station-keeping analysis on a Sun–Earth $L_1$ quasi-halo trajectory

##### 4.1. Initial guess formulation

As seen in Section 3, a good initial guess is essential for the I-MPSP algorithm to have fewer iterations and faster convergence. Consider a scenario in which  $n$  station-keeping maneuvers are executed to drive the spacecraft to its reference orbit, as seen in Fig. 3. The guessed station-keeping maneuvers can be obtained using state transition matrices (STMs). The final deviation of the spacecraft  $\Delta X_{N,n}$  as a function of initial condition deviation  $\Delta X_{N,0}$  from the reference orbit and station-keeping maneuvers  $\Delta V_j, j = 1, 2, \dots, n$  can be written using STMs as

$$\Delta X_{N,n} = \Phi(t_f, t_0) \Delta X_{N,0} + \bar{A} \begin{bmatrix} \Delta V_1 \\ \Delta V_2 \\ \vdots \\ \Delta V_n \end{bmatrix} \quad (37)$$

where

$$\bar{A} = \begin{bmatrix} \Phi(t_f, t_{U_1})_{C_4:C_6} & \Phi(t_f, t_{U_2})_{C_4:C_6} & \cdots & \Phi(t_f, t_{U_n})_{C_4:C_6} \end{bmatrix}$$

$\Phi(t_f, t_0)$  represents the STM calculated on the reference orbit from time  $t_0$  to  $t_f$ .  $\Phi(t_f, t_{U_j})_{C_4:C_6}, j = 1, 2, \dots, n$  represents the last three columns of STM from time  $t_{U_j}$  to  $t_f$ . The guessed maneuver history that takes the final deviation  $\Delta X_{N,n}$  to zero is then obtained as

$$\begin{bmatrix} \Delta V_1 \\ \Delta V_2 \\ \vdots \\ \Delta V_n \end{bmatrix} = \bar{A}^+ \left\{ -\Phi(t_f, t_0) \Delta X_{N,0}^0 \right\}, \bar{A}^+ = \bar{A}^T (\bar{A} \bar{A}^T)^{-1} \quad (38)$$

Integrating the non-linear system dynamics using the guessed station-keeping control values drives the spacecraft close to the desired final condition. The remaining deviation is reduced by the I-MPSP controller in an iterative manner.

##### 4.2. Station-keeping with nominal dynamics and initial condition variation

The station-keeping guidance algorithm developed in the previous section will be verified under nominal conditions. This will be done by targeting a spacecraft with large initial condition errors to the desired location on the reference quasi-halo orbit. Except for errors in the initial condition of the spacecraft, uncertainty in orbit determination and SRP errors are assumed to be zero. At the time of station-keeping maneuver, states are updated using Eq. (8) and nominal dynamics Eqs. (1)–(6) are used for spacecraft propagation. Several initial conditions are chosen by perturbing each component of the initial state  $O$  on the quasi-halo orbit. The variation in states follow a uniform distribution as shown in Table 2. Without any station-keeping maneuvers, the perturbed initial conditions, when propagated using nominal dynamics, quickly diverge from the reference orbit and escape the  $L_1$  region as shown in Fig. 4(a). In Fig. 4(b), a sequence of  $n = 2$  station-keeping maneuvers computed using the I-MPSP algorithm successfully drive all the initial conditions to the target state  $X^*$  on the reference orbit. The duration for station-keeping guidance  $T = \frac{p}{2}$  was chosen to be half a revolution of the quasi-halo orbit. The first maneuver  $\Delta V_1$  are performed at initial time  $t_0$ , followed by the remaining maneuver  $\Delta V_2$  separated by a time interval of  $\frac{T}{2} \approx 45$  days. Depending upon the magnitude of deviation in initial conditions, the algorithm takes two to three iterations to converge to the terminal state  $X^*$ . The error constraint for terminal position and velocity components were set as 1.5 km and  $3 \times 10^{-4}$  m/s, respectively. A sample iteration history for a particular initial condition with an error  $-5 \times 10^4$  km and  $-5$  m/s along all position and velocity components is shown in Fig. 6(a). The initial condition, when propagated without any station-keeping maneuvers, immediately escapes

**Table 2**

Initial condition errors.

Error in state $\bar{X}_{N_0}$ at $t_0$	Distribution
$\Delta x, \Delta y, \Delta z$	$U(-5 \times 10^4, 5 \times 10^4)$ km
$\Delta v_x, \Delta v_y, \Delta v_z$	$U(-5, 5)$ m/s

**Table 3**

Terminal output error evolution using I-MPSP.

Error	Zero control	Guess	Iter 1	Iter 2
$ \Delta x_{N,n} $ km	$6.9 \times 10^5$	$1.1 \times 10^4$	$4.6 \times 10^1$	$5.2 \times 10^{-2}$
$ \Delta y_{N,n} $ km	$7.3 \times 10^5$	$8.9 \times 10^3$	$9.4 \times 10^0$	$3.0 \times 10^{-2}$
$ \Delta z_{N,n} $ km	$2.3 \times 10^4$	$9.6 \times 10^2$	$3.5 \times 10^0$	$2.0 \times 10^{-3}$
$ \Delta \dot{x}_{N,n} $ m/s	$2.8 \times 10^2$	$6.4 \times 10^0$	$6.1 \times 10^{-2}$	$3.0 \times 10^{-5}$
$ \Delta \dot{y}_{N,n} $ m/s	$3.2 \times 10^2$	$4.5 \times 10^0$	$5.0 \times 10^{-4}$	$2.0 \times 10^{-5}$
$ \Delta \dot{z}_{N,n} $ m/s	$8.3 \times 10^0$	$3.3 \times 10^{-2}$	$1.5 \times 10^{-3}$	$2.2 \times 10^{-6}$
$\ \Delta X_{N,n}(1 : 3)\ $ km	$1.0 \times 10^6$	$1.4 \times 10^4$	$4.7 \times 10^1$	$6.0 \times 10^{-2}$
$\ \Delta X_{N,n}(4 : 6)\ $ m/s	$4.3 \times 10^2$	$7.8 \times 10^0$	$6.1 \times 10^{-2}$	$3.6 \times 10^{-5}$

**Table 4**

Terminal output error — Floquet and TPA approaches.

Error	Floquet mode	TPA
$ \Delta x_{N,n} $ km	$1.3 \times 10^4$	$1.8 \times 10^4$
$ \Delta y_{N,n} $ km	$3.7 \times 10^4$	$1.8 \times 10^4$
$ \Delta z_{N,n} $ km	$3.8 \times 10^4$	$1.3 \times 10^4$
$ \Delta \dot{x}_{N,n} $ m/s	$1.7 \times 10^0$	$6.8 \times 10^0$
$ \Delta \dot{y}_{N,n} $ m/s	$1.2 \times 10^1$	$6.3 \times 10^0$
$ \Delta \dot{z}_{N,n} $ m/s	$6.1 \times 10^0$	$7.8 \times 10^{-1}$
$\ \Delta X_{N,n}(1 : 3)\ $ km	$5.5 \times 10^4$	$2.9 \times 10^4$
$\ \Delta X_{N,n}(4 : 6)\ $ m/s	$1.4 \times 10^1$	$9.3 \times 10^0$

**Table 5**

I-MPSP computational time.

Initial Guess (s)	Iteration 1 (s)	Iteration 2 (s)	Total time (s)
0.2	0.15	0.15	0.8

the  $L_1$  region. By utilizing an informed initial guess for the station-keeping maneuvers as shown in Section 4.1, the I-MPSP algorithm was able to converge in two iterations. The evolution of terminal output error  $\Delta Y_{N,n}$  corresponding to Fig. 6(a) is shown in Table 3. Table 5 indicates the time taken to generate the initial guess and perform all iterations to achieve convergence. Further computational details are described in detail in Section 4.5. In the absence of disturbance forces and uncertainties, upon reaching the target location on the reference orbit, the spacecraft will continue to remain on it.

A comparison with the Floquet mode approach [10–12] and the target point approach [13–15] was performed using the same set of deviated initial conditions and the resulting trajectories are shown in Figs. 5(a) and 5(b), respectively. The theory and implementation procedure behind the Floquet mode approach is described briefly with appropriate references in Appendix A. The target point approach is formulated to be equivalent to the I-MPSP technique and is described briefly in Appendix B. Although both the techniques correct the initial conditions in the right direction, at the end of the guidance time, the resulting trajectories have a significant deviation from the desired final condition  $X^*$ . For a particular initial condition with an error  $-5 \times 10^4$  km and  $-5$  m/s along all position and velocity components, the resulting terminal state error in both the techniques is shown in Table 4. The presence of a large residual error at the end of the guidance time results in the trajectories quickly deviating from the nominal orbit upon propagation beyond the guidance time as seen in Fig. 6(b). Both the Floquet mode and target point approach are formulated based on a linear approximation of spacecraft dynamics around the reference orbit. Hence, these methods are not effective for large spacecraft deviations.

#### 4.3. Disturbance forces and mission uncertainties

The nominal spacecraft equations of motion in the E4BP as described in Section 2.2 are based on certain simplified assumptions. In

a realistic scenario, the spacecraft is subjected to unknown disturbance forces and uncertainties associated with the mission. The actual magnitude of the SRP force will be different from the nominal value due to the uncertainty associated with the coefficient of reflectivity, which is modeled using a uniform distribution as indicated in Table 6.

Other significant uncertainties associated with a halo orbit mission include spacecraft orbital injection and orbit determination errors. Orbital injection errors induce a change in spacecraft initial conditions at the beginning of the mission. This initial deviation, when left unchecked, will cause the spacecraft to permanently escape the  $L_1$  region due to the unstable nature of the reference trajectory. To emulate a realistic station-keeping mission scenario, orbital injection errors are modeled using uniform distribution as shown in Table 6. In an ideal scenario when the state-feedback of the spacecraft is accurate, the station-keeping control will precisely re-target the deviated spacecraft to the reference trajectory. But in practice, an orbit determination process to estimate the spacecraft states always involves a certain amount of uncertainty. This leads to a slight inaccuracy in the computation of station-keeping control. Orbit determination errors in this work are modeled using uniform distribution as shown in Table 6. The various uncertainties used in this work have been previously employed in [18, 20, 28] to evaluate different station-keeping guidance techniques.

#### 4.4. Propagation model for the spacecraft

While nominal spacecraft dynamics are used for station-keeping control computation, the propagation model incorporates unknown disturbances and uncertainties associated with a practical mission. As described in the previous Section 4.3, due to errors in the coefficient of reflectivity, the actual SRP force in  $S$  frame is

$$a_{srp} = \frac{S_M \|\bar{r}_{s-e}\|^2 C_r A_{srp}}{m_{s/c} \|\bar{r}_{s-s/c}\|^2 c} \hat{r}_{s-s/c} \quad (39)$$

where  $C_r$  represents the actual coefficient of reflectivity.

While formulating the station-keeping controller, maneuver implementation is modeled as an instantaneous change in spacecraft velocities as shown in Eq. (8). In a practical scenario, thrusters provide the necessary velocity change by firing for a small, finite duration. This phenomenon is implemented in the propagation model. The spacecraft is assumed to be fully controllable along all the three axes in the  $S$  frame having a constant thrust value  $|\tilde{\tau}_x| = |\tilde{\tau}_y| = |\tilde{\tau}_z| = 10$  N. The duration for station-keeping maneuver execution along each axis is obtained using the Tsiolkovsky rocket equation [29]

$$t_{sk} = g_0 I_{sp} m_o \frac{\left(1 - e^{-\frac{\Delta V}{I_{sp} g_0}}\right)}{|\tilde{\tau}|} \quad (40)$$

where  $m_0$  is the mass of the spacecraft before maneuver execution,  $g_0$  is the acceleration due to gravity on Earth,  $I_{sp}$  is the specific impulse of the engine,  $|\tilde{\tau}|$  is the constant thrust value and  $t_{sk}$  is the execution time to impart  $\Delta V$  magnitude of spacecraft velocity as computed by the station-keeping controller in the synodic frame. Thrust acceleration along the appropriate directions in  $S$  frame is incorporated into Eqs. (4)–(6) as

$$a_T = \frac{1}{m_{s/c}} \begin{bmatrix} \tilde{\tau}_x \\ \tilde{\tau}_y \\ \tilde{\tau}_z \end{bmatrix} \quad (41)$$

Upon calculating maneuver execution times, the thrust along each axis is switched on for a time  $0 < t < t_{sk}$  and fired in an open-loop sense to deliver the station-keeping velocity requirement.

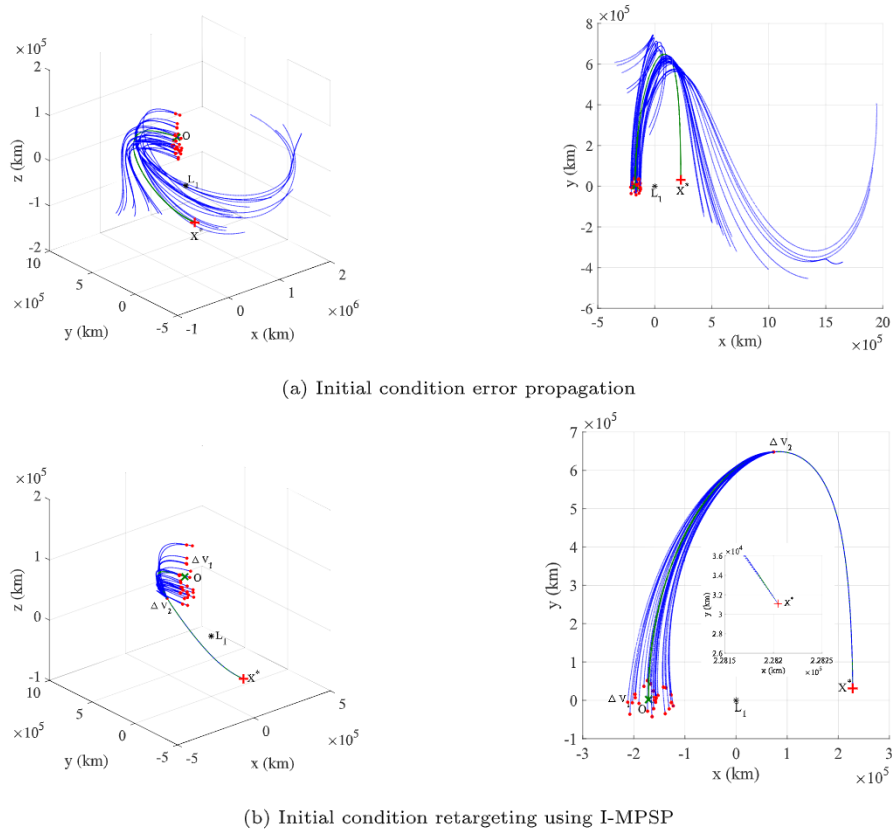


Fig. 4. Large initial condition error correction using I-MPSP.

**Table 6**

Uncertainty in simulation parameters [18,20,28].

Parameter	Distribution
Orbit Injection/Determination Error — Position km	$U_x(-9, 9)$ , $U_y(-90, 90)$ , $U_z(-90, 90)$
Orbit Injection/Determination Error — Velocity mm/s	$U_x(-45, 45)$ , $U_y(-45, 45)$ , $U_z(-90, 90)$
Reflectivity Coefficient Error Percentage	10%

#### 4.5. Long duration station-keeping using the I-MPSP strategy

Due to the various uncertainties, the station-keeping maneuvers computed using the nominal model will not drive the spacecraft precisely to the target state on the reference trajectory. The residual error will eventually accumulate and cause the spacecraft to escape the  $L_1$  region. To keep the spacecraft close to the reference orbit, station-keeping maneuvers must be executed on a periodic basis. Hence the I-MPSP controller is implemented in a closed-loop manner to keep a spacecraft around the reference quasi-halo orbit for five years. The closed-loop implementation of the I-MPSP controller is illustrated in Fig. 7. Maneuvers executed for orbital insertion will not be a part of the station-keeping cost. Controller parameters that include station-keeping guidance time  $T$ , number of maneuvers  $n$  and values for the weight matrices are set at the beginning of the simulation.

For all the simulations, equal weights have been assigned to all the components of station-keeping control variables, and hence the weight matrices  $R_j, j = 1, 2, \dots, n$  are considered to be identity matrices. The tolerance value for terminal output translates to 1.5 km and  $3 \times 10^{-4}$  m/s in position and velocity, respectively. It is a common practice to choose one halo orbit  $P$  time as the guidance time-period [18–20] and the same has been considered in this work. The presence of navigational errors results in large downstream state deviations when the guidance time is chosen to be very large. Whereas a shorter guidance time leads to higher station-keeping costs due to aggressive corrections. The spacecraft parameters used for the simulation are

given in Table 7. As the uncertainties in the dynamical system have a stochastic nature, multiple simulations are performed to estimate the mean value of total station-keeping cost as well as to quantify the deviation from the reference trajectory. The total station-keeping cost incurred by the spacecraft is the summation of the individual station-keeping maneuvers executed during its mission duration. For a particular set of station-keeping parameters, the total station-keeping cost varies with each simulation as the sequence of random numbers that generate various uncertainties change in each simulation. Hence, the mean value of the total station-keeping cost computed over the entire simulations will result in a good estimate of the station-keeping cost for the mission.

Two different scenarios are simulated with parameters shown in Table 8. In scenarios A and B, the number of maneuvers  $n$  executed in each guidance time is set to two and three, respectively. This corresponds to a station-keeping maneuver performed every ninety days in scenario A and sixty days in scenario B, respectively. The evolution of the mean and standard deviation of the cumulative station-keeping cost over five years and 200 simulations is shown in Fig. 8. The mean and standard deviation of the position error of the spacecraft during maneuver execution is shown in Fig. 9. A sample trajectory of the spacecraft and the mean value of individual station-keeping maneuvers is shown in Fig. 10. Note that, in both the scenarios, the mean value of position error is much less compared to the dimension of the quasi-halo orbit. The position errors in scenario B is less compared to A due to the increase in the frequency of station-keeping maneuvers.

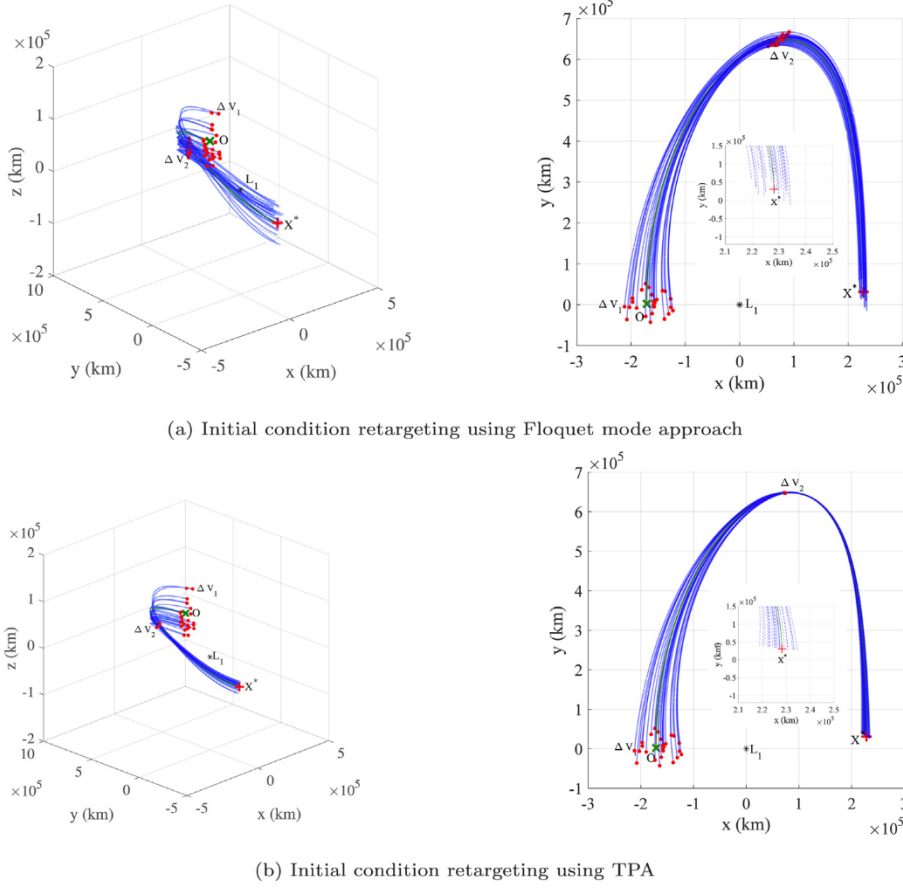


**Fig. 5.** Large initial condition error correction using Floquet mode and target point approach.

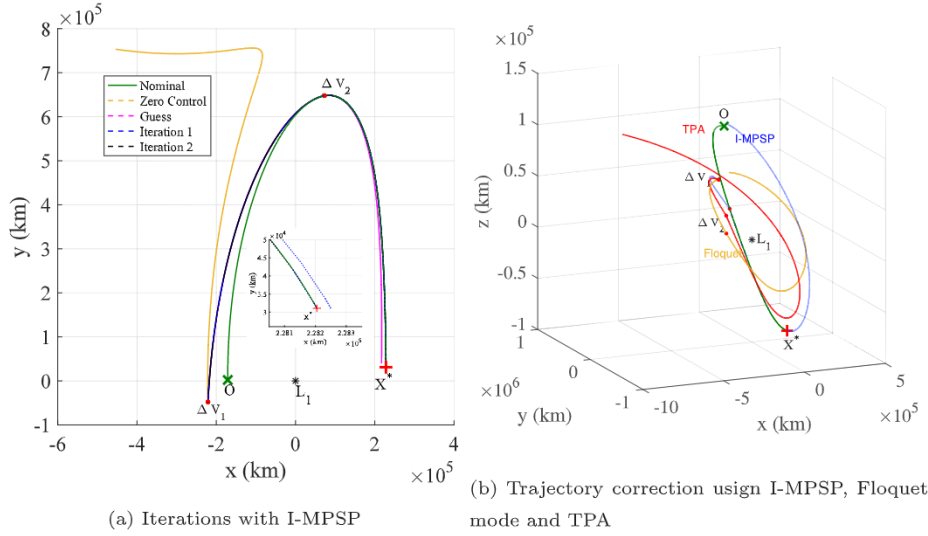


**Fig. 6.** Initial condition re-targeting using I-MPSP, Floquet mode and TPA.

A comparative analysis using the Floquet mode approach is performed for both scenarios. In order for the analysis to be fair, the maneuver execution times, as well as the random uncertainties are chosen to be the same values as the I-MPSP simulations. The orbit injection, orbit determination and reflectivity coefficients for all the 200 I-MPSP simulations are saved and used in the same sequence during the Floquet mode controller implementation. The resulting mean and standard deviation of the position error of the spacecraft is shown in Fig. 9. It

is known that existing station-keeping techniques result in a linear position divergence from the reference trajectory during a long-duration mission [18–20]. Similar behavior is found in the simulations carried out using Floquet mode controller. A key observation to be noted is that in addition to the mean of the position error, the standard deviation also increases with time. For a long duration halo orbit mission, apart from the station-keeping cost, the position error of the spacecraft from the nominal orbit is equally important. For missions involving precise

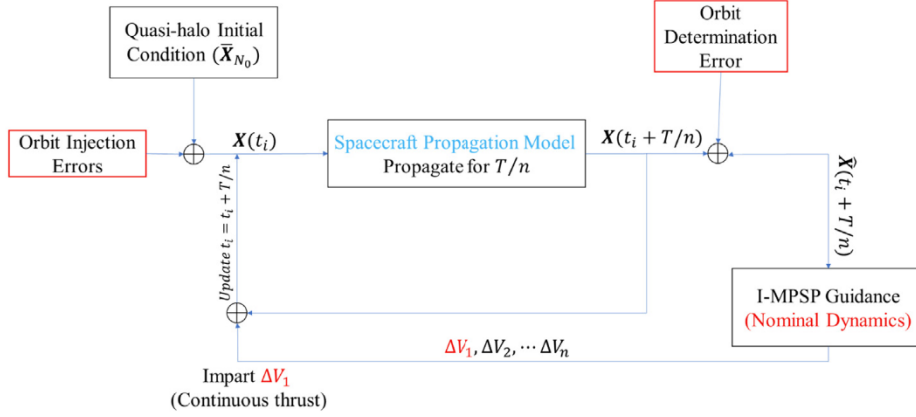
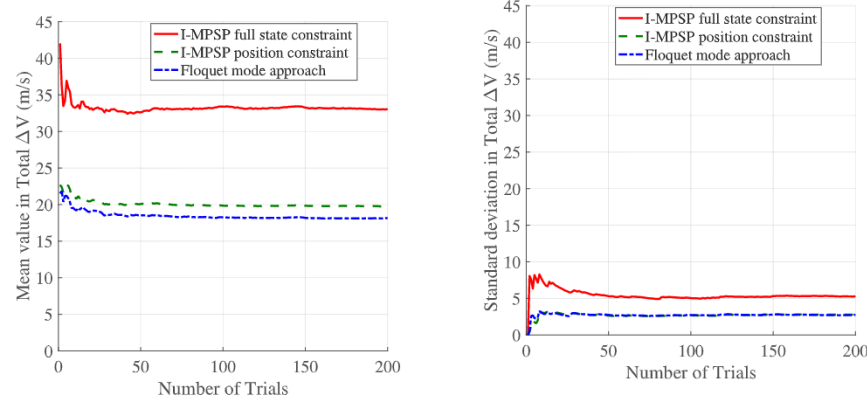
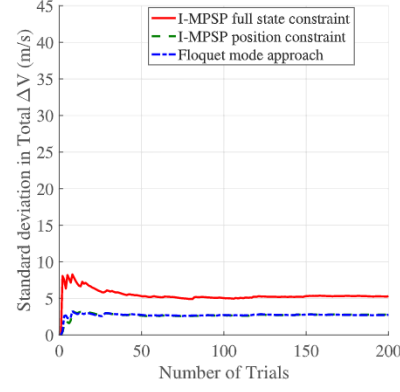


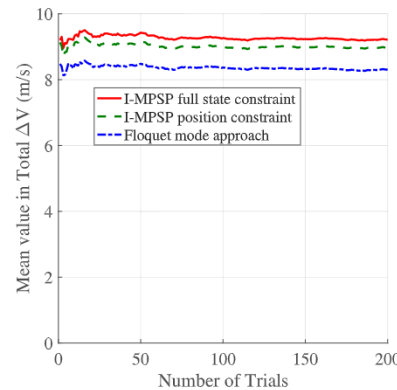
Fig. 7. Closed loop I-MPSP implementation.



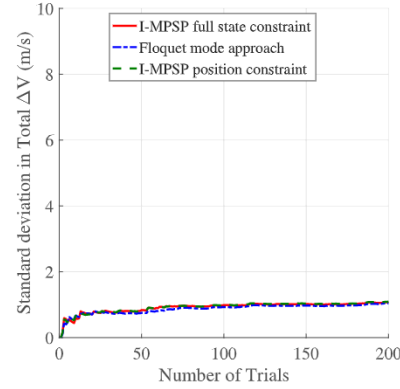
(a) Type A - Mean value of cumulative station-keeping cost for five years averaged over trials



(b) Type A - Standard deviation in cumulative station-keeping cost for five years averaged over trials



(c) Type B - Mean value of cumulative station-keeping cost for five years averaged over trials



(d) Type B - Standard deviation in cumulative station-keeping cost for five years averaged over trials

Fig. 8. Evolution of the mean and standard deviation of total station-keeping cost for five years.

observation requirement or space crafts in a formation flying configuration on multiple nearby reference trajectories, a tighter trajectory is desired. Similar to the Floquet mode approach, the target point approach also resulted in a position divergence of the spacecraft; however, the deviation depended on tuning the weighting matrix in the cost function associated with the state deviation at the target point. In all

the simulations, the spacecraft position errors resulting from the I-MPSP controller were found to be lesser than the target point approach.

The application of the I-MPSP controller results in a trajectory with almost a constant position error, i.e., a near-zero divergence rate, for the entire mission duration. This is because the I-MPSP controller ensures that the terminal state constraints are accurately met

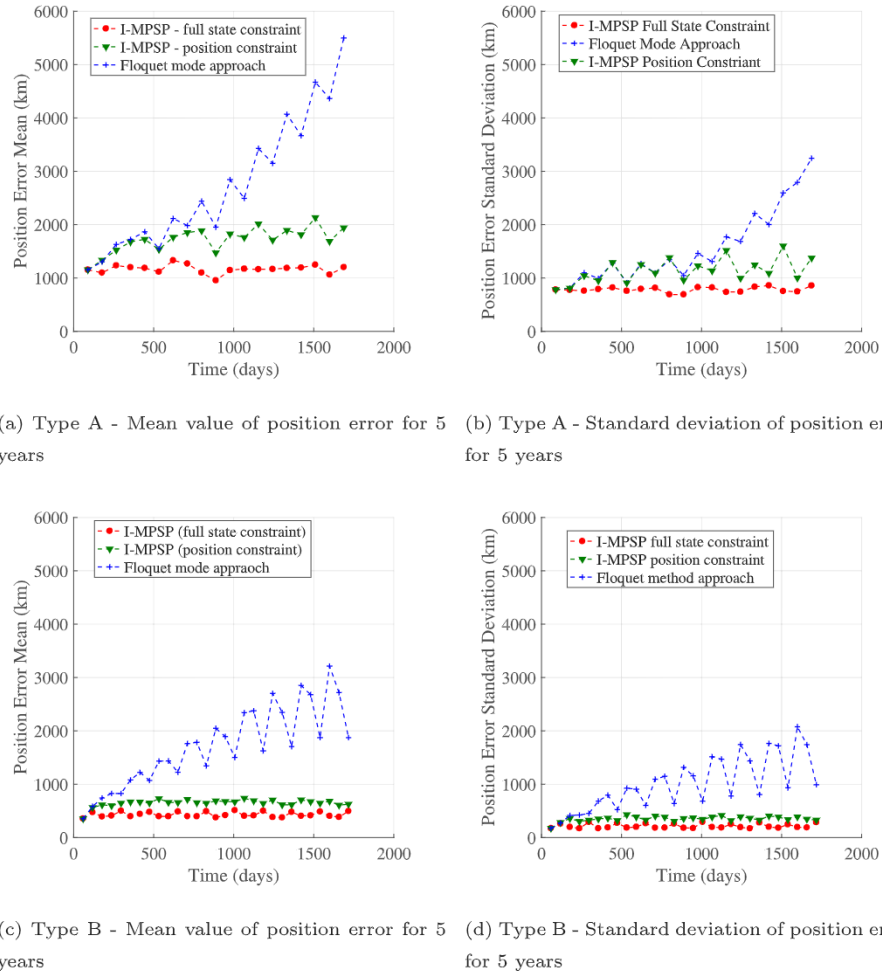


Fig. 9. Mean and standard deviation of spacecraft position error from reference orbit at the time of maneuver execution.

**Table 7**  
Spacecraft and SRP parameters.

Spacecraft mass	Area	$\bar{C}_r$	Isp	$c$	$S_M$
500 kg	3 m <sup>2</sup>	1.5	330 s	$3 \times 10^8$ m/s	1358 W/m <sup>2</sup>

during the computation of a station-keeping maneuver. The ability to maintain a tighter trajectory around the reference orbit comes at the cost of increased station-keeping cost compared to the Floquet mode approach. However, it is interesting to observe in Fig. 9 that by formulating a terminal position constraint, instead of a full state constraint, the station-keeping cost can be reduced with a slight increase in the position errors. The mean and standard deviation of the annual station-keeping costs in both the scenarios is given in Table 9. The station-keeping costs estimated in this work fall in the range of values obtained by other works [18,20,28] that used similar uncertainty levels. Incorporating a terminal output constraint (full state or position) in the station-keeping guidance formulation significantly reduces the spacecraft position errors and prevents the drift from the nominal orbit over a long-duration mission.

The I-MPSP controller is a computational guidance technique in which the number of iterations and the convergence time are important to evaluate its performance. The computational cost incurred by the I-MPSP controller to carry out 3800 station-keeping maneuvers over 200 simulations of the Type A scenario is depicted in Fig. 11. A histogram of the number of iterations to achieve convergence for a maneuver

**Table 8**  
Parameters for I-MPSP station-keeping guidance.  $P = 178$  days is halo time period.

Parameter	Type A	Type B
$T$	$P$	$P$
$n$	2	3
$N$	26	21

**Table 9**  
Annual station-keeping cost averaged over 200 trials.

Simulation type	Controller	Mean $\Delta V$ (m/s)	Standard deviation (m/s)
A	I-MPSP (full state constraint)	6.6	1.1
A	I-MPSP (position constraint)	3.9	0.6
A	Floquet mode	3.6	0.6
B	I-MPSP (full state constraint)	1.9	0.2
B	I-MPSP (position constraint)	1.8	0.2
B	Floquet mode	1.7	0.2

computation is shown in Fig. 11(b). The majority of the station-keeping maneuvers take less than three iterations. The convergence time for station-keeping maneuver computation is shown in Fig. 11(c). The I-MPSP controller takes less than half a second for majority of station-keeping maneuvers. For all the simulations, the solver is run on an 8GB RAM Intel(R) Core(TM) i7-7500U processor @ 2.70 GHz, in the Matlab 9.1.0.441655 (R2016b) simulation environment. Note that the

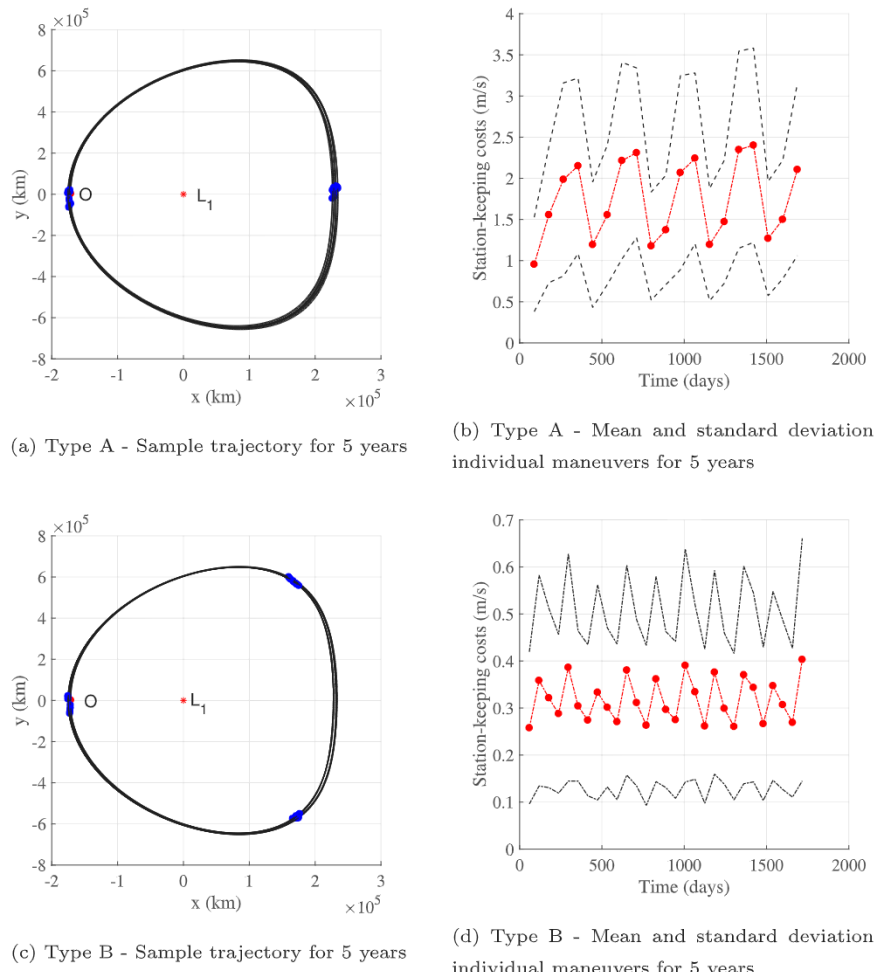


**Fig. 10.** Sample spacecraft trajectory, mean and standard deviation for station-keeping maneuvers for five years.

computational time will further reduce upon coding the algorithm on an embedded platform, and several advanced space-grade processors [30] are currently under development to enable real-time onboard computation of the guidance command. The computational efficiency of MPSP based guidance schemes and their applicability for onboard autonomous guidance implementation is documented in [31,32]. The computational time window being very large (time between two maneuvers is in the order of days), the technique can also be used in the traditional way of ground station implementation after receiving the telemetry data.

## 5. Conclusion

In this paper, I-MPSP, a computationally efficient, optimal control strategy, is applied to regulate a spacecraft around an  $L_1$  quasi-halo orbit in the Sun–Earth–Moon elliptic four-body problem. The station-keeping requirement is modeled as a finite-time, non-linear optimal control problem with hard terminal output constraints. The algorithm is iterative and requires an initial control guess history. A state transition matrix-based approach is used to provide an informed initial guess for the station-keeping algorithm. Under nominal conditions with large errors in the initial state, the I-MPSP guidance effectively redirects the spacecraft to the reference trajectory and satisfies the terminal output constraint accurately. For a long duration of orbital maintenance, all the simulations are performed under realistic conditions that include an SRP disturbance force and uncertainties in mission parameters such as orbit insertion and orbit determination errors. Compared to the

traditional station-keeping methodologies, application of the I-MPSP controller in a closed loop manner results in a trajectory with an almost constant position error, i.e., a near-zero divergence rate, for the entire mission duration.

## Declaration of competing interest

The authors declare that they have no known competing financial interests or personal relationships that could have appeared to influence the work reported in this paper.

## Appendix A. Floquet mode approach

The Floquet mode approach is an alternate strategy to maintain a spacecraft near a reference libration point orbit. First appearing in the works of Kogan [10], Simó et al. [11] and Gómez et al. [12], FMA uses the information about the dynamical flow of the phase space along the periodic orbit in order to calculate a station-keeping maneuver. At any time  $t_0$ , the state of the spacecraft has a certain deviation  $\Delta X(t_0)$  from the nominal orbit. At a future time  $t$ , a linear approximation to the deviation of the state can be obtained using the state transition matrix  $\Phi(t, t_0)$  as follows

$$X(t) = \Phi(t, t_0) X(t_0) \quad (\text{A.1})$$

The STM at any point along the trajectory is computed by integrating the variational equations of motion along the nominal orbit

$$\dot{\Phi}(t, t_0) = A(t) \Phi(t, t_0) \quad (\text{A.2})$$

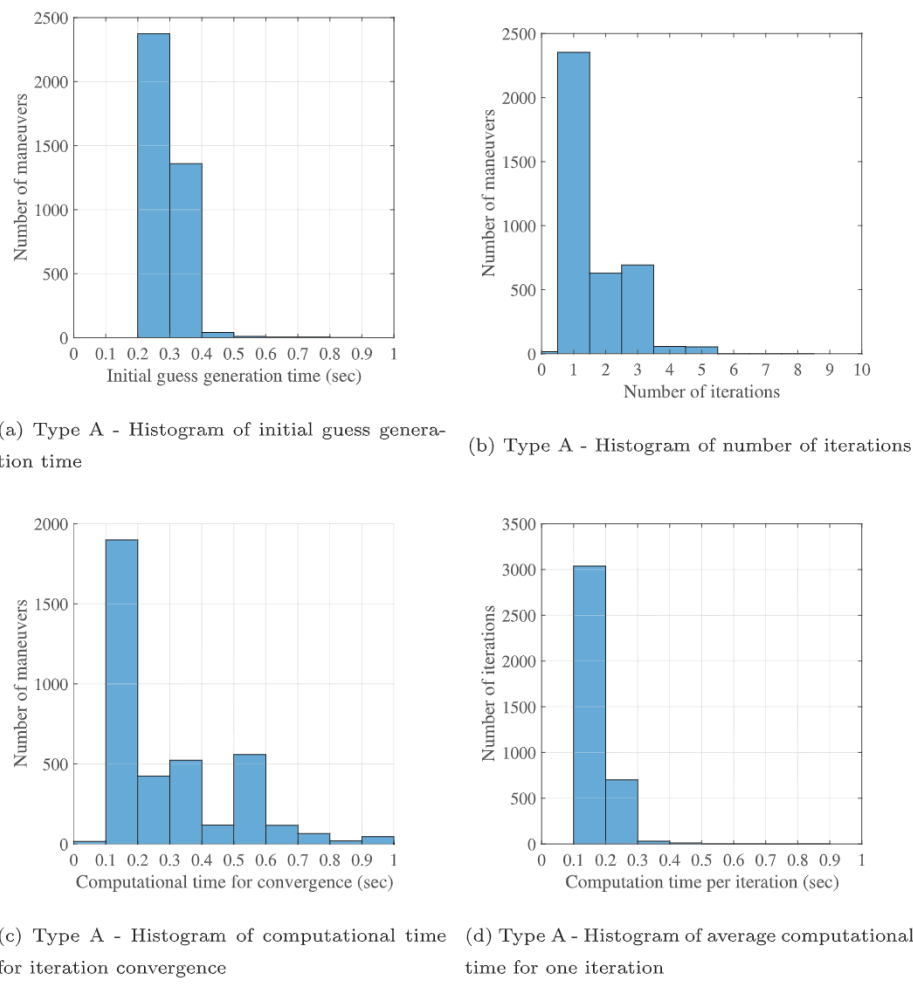


**Fig. 11.** Computational cost incurred by the I-MPSP controller for Type A simulations.

For a nominal orbit with a periodic Jacobian matrix  $A(t)$ , such as a halo orbit of period  $P$ , the STM is decomposed into its eigenstructure at time  $t$  using the Floquet theorem [19]

$$\Phi(t, t_0) = F(t)e^{Y(t-t_0)}F^{-1}(t_0) \quad (\text{A.3})$$

where  $F(t)$  is the periodic, non-singular Floquet modal matrix of period  $P$  and  $Y$  is a diagonal matrix. The columns of matrix  $F(t_0)$  are the set of eigenvectors and  $e^{YP}$  is a diagonal matrix comprising the eigenvalues of the monodromy matrix  $\Phi(t_0 + P, t_0)$ . In this paper, the nominal quasi-halo orbit in the E4BP is nearly periodic compared to the exactly periodic halo orbit in the CR3BP model. This leads to the following eigenvalue structure for the monodromy matrix. Two of the eigenvalues are real and exist as a reciprocal pair. The first eigenvalue  $\lambda_1 > 1$  and the eigenvector  $F_{(:,1)}(t_0)$  correspond to the unstable direction. The second eigenvalue  $\lambda_2 = \frac{1}{\lambda_1} < 1$  and the eigenvector  $F_{(:,2)}(t_0)$  correspond to the stable direction. The unstable and stable Poincaré exponents, are obtained as  $Y_{j,j} = \frac{\ln(\lambda_j)}{P}$ ,  $j = 1, 2$ . The remaining eigenvalues form two sets of complex conjugate pairs and the corresponding eigenvectors represent oscillatory behavior. For an eigenvalue pair  $\lambda_j = a \pm ib = \sigma e^{\pm i\theta}$ ,  $j = 3, 4$ , where  $\sigma = \sqrt{a^2 + b^2}$ ,  $\theta = \tan^{-1}(b/a)$ , the corresponding Poincaré exponents are  $Y_{j,j} = \frac{\ln(\sigma e^{\pm i\theta})}{P}$ ,  $j = 3, 4$ . The Poincaré exponents  $Y_{j,j}$ ,  $j = 5, 6$  for the last eigenvalue pair are found in a similar way. The matrix  $F(t)$  whose columns represent the Floquet modes along the nominal orbit are obtained as

$$F(t) = \Phi(t, t_0)F(t_0)e^{-Y(t-t_0)} \quad (\text{A.4})$$

By representing the Floquet modes, i.e the columns of matrix  $F(t)$  as  $f_j(t)$ ,  $j = 1, 2, \dots, 6$ , at any given time  $t$ , the deviation of the spacecraft

state  $\Delta X(t)$  is written in terms of the Floquet basis as

$$\Delta X(t) = \sum_{j=1}^6 c_j f_j(t) \quad (\text{A.5})$$

As  $f_1$  represents the unstable direction, a non-zero projection component  $c_1$  leads to the spacecraft's exponential divergence from the nominal orbit. Therefore, the Floquet mode station-keeping strategy seeks to perform a maneuver that cancels the unstable component  $c_1$  [33,34]. The unstable component of motion  $c_1$  is obtained as

$$c_1 = \frac{\det(\Delta X(t), f_2(t), \dots, f_6(t))}{\det(f_1(t), \dots, f_6(t))} = \langle \pi^1(t), \Delta X(t) \rangle \quad (\text{A.6})$$

The components of  $\pi^1(t) = [\pi_1^1(t), \dots, \pi_6^1(t)]^T$  are called the projection factors along the unstable direction. Thus, the component along the unstable Floquet mode  $c_1$  is just the dot product between  $\pi^1(t)$  and state deviation  $\Delta X(t)$ . In order to cancel the unstable component, a station-keeping maneuver  $\Delta V(t)$  is executed such that the dot product vanishes, i.e.

$$\left\langle \pi^1(t), \left( \Delta X(t) + \begin{bmatrix} 0_{3 \times 3} \\ \Delta V(t) \end{bmatrix} \right) \right\rangle = 0 \quad (\text{A.7})$$

A solution that minimizes the  $\Delta V^T(t)Q\Delta V(t)$  is obtained and given by

$$\Delta V = -Q^{-1}B^T(BQ^{-1}B^T)^{-1}c_1 \quad (\text{A.8})$$

where  $B = [\pi_4^1(t), \pi_5^1(t), \pi_6^1(t)]^T$ . Minimizing the control effort while calculating the station-keeping maneuver ensures consistency during comparison with the previous strategies.

## Appendix B. Target point approach

The target point approach (TPA) and its variations [13–15], was proposed by Howell et al. [16] as a station-keeping strategy for libration point orbits. In this approach, optimal station-keeping maneuvers are obtained by minimizing a predefined cost function, that is a combination of the applied station-keeping maneuvers and the deviation of the spacecraft state from the nominal trajectory at a desired future time. In this paper, the following cost function for TPA is formulated to be equivalent to the I-MPSP guidance used in Sections 4.2 and 4.5.

$$\min_{\Delta V_1, \Delta V_2} J = \Delta V_1^T Q_1 \Delta V_1 + \Delta V_2^T Q_2 \Delta V_2 + \Delta X^T(t_f) R_f \Delta X(t_f) \quad (\text{B.1})$$

where,  $\Delta V_1$  and  $\Delta V_2$  represent the station-keeping maneuvers performed at times  $t_1$  and  $t_2$ , respectively. The predicted deviation of the spacecraft from the nominal orbit at a future target time  $t_f$  is represented by  $\Delta X(t_f)$ .  $Q_1$ ,  $Q_2$  and  $R_f$  represent the weighting matrices for the two station-keeping maneuvers and the predicted deviation, respectively. The state transition matrices corresponding to the linearized spacecraft dynamics, are used to express the future deviation  $\Delta X(t_f)$  in terms of station-keeping maneuvers and initial deviation  $\Delta X(t_1)$ :

$$\Delta X(t_f) = \Phi(t_f, t_2) \left( \Delta X(t_2) + \begin{bmatrix} 0_{3 \times 3} \\ \Delta V_2 \end{bmatrix} \right) \quad (\text{B.2})$$

$$\Delta X(t_2) = \Phi(t_2, t_1) \left( \Delta X(t_1) + \begin{bmatrix} 0_{3 \times 3} \\ \Delta V_1 \end{bmatrix} \right) \quad (\text{B.3})$$

$\Phi(t_j, t_i)$  represents the STM computed along the nominal orbit from time  $t_i$  to  $t_j$ , respectively.  $\Delta X(t_1)$  and  $\Delta X(t_2)$  represent the deviation of the spacecraft state from the nominal orbit just before the execution of station-keeping maneuvers. The necessary conditions for optimality of equation lead to the following station-keeping maneuvers:

$$\Delta V_1 = \Pi^{-1} \beta \quad (\text{B.4})$$

$$\Delta V_2 = (\Lambda_2^T R_f \Gamma_2)^{-1} \left( -(\Lambda_1 \Lambda_2^T R_f \Lambda_2) \Delta V_1 - \Lambda_2^T R_f \Phi(t_f, t_1) \Delta X(t_1) \right) \quad (\text{B.5})$$

$\Pi$  and  $\beta$  are

$$\Pi = \Gamma_2^T R_f \Lambda_2 - (\Lambda_2 + \Gamma_2^T R_f \Gamma_2) (\Lambda_2^T R_f \Gamma_2)^{-1} (\Lambda_1 + \Lambda_2^T R_f \Lambda_2) \quad (\text{B.6})$$

$$\beta = (\Lambda_2 + \Gamma_2^T R_f \Gamma_2) (\Lambda_2^T R_f \Gamma_2)^{-1} \left( \Lambda_2^T R_f \Phi(t_f, t_1) \Delta X(t_1) - \Gamma_2^T R_f \Phi(t_f, t_1) \Delta X(t_1) \right) \quad (\text{B.7})$$

$\Lambda_1$ ,  $\Lambda_2$ ,  $\Gamma_1$  and  $\Gamma_2$  are obtained from the columns of STM as

$$\Lambda_1 = \Phi(t_f, t_1)_{C_1:C_3}, \Lambda_2 = \Phi(t_f, t_1)_{C_4:C_6} \quad (\text{B.8})$$

$$\Gamma_1 = \Phi(t_f, t_2)_{C_1:C_3}, \Gamma_2 = \Phi(t_f, t_2)_{C_4:C_6} \quad (\text{B.9})$$

This way of formulating the cost function ensures uniformity while evaluating its performance against the I-MPSP technique. Although the target point approach is a simple and robust method, its ability to maintain the spacecraft close to the nominal orbit greatly depends upon appropriate selection of the weighting matrices.

## References

- [1] M. Shirobokov, S. Trofimov, M. Ovchinnikov, Survey of station-keeping techniques for libration point orbits, *J. Guid. Control Dyn.* 40 (5) (2017) 1085–1105.
- [2] A. Narula, J. Biggs, Fault-tolerant station-keeping on libration point orbits, *J. Guid. Control Dyn.* 41 (4) (2018) 879–887.
- [3] Y. Akiyama, M. Bando, S. Hokamoto, Explicit form of station-keeping and formation flying controller for libration point orbits, *J. Guid. Control Dyn.* 41 (6) (2018) 1407–1415.
- [4] Y. Akiyama, M. Bando, S. Hokamoto, Station-keeping and formation flying based on nonlinear output regulation theory, *Acta Astronaut.* 153 (2018) 289–296.
- [5] S. Jung, Y. Kim, Hamiltonian structure-based robust station-keeping for unstable libration point orbits, *J. Guid. Control Dyn.* 42 (9) (2019) 1912–1929.
- [6] M. Lidov, S. Lukianov, Statistical estimates in the control problem for motion of a space vehicle in the vicinity of a collinear libration point, *Cosm. Res.* 14 (6) (1977) 922–935.
- [7] M. Lidov, V. Lyakhova, The guaranteeing synthesis of control for stabilization of the motion of a space vehicle in the vicinity of unstable libration points, *Kosmicheskie Issledovaniia* 30 (5) (1992) 579–595.
- [8] I. Ilyin, Quasi-periodic orbits around Sun-Earth L2 libration point and their transfer trajectories in Russian space missions (Ph.D. thesis), Keldysh Institute of Applied Mathematics of RAS, Moscow, 2015.
- [9] P. El'yasberg, T. Timokhova, Control of spacecraft motion in neighborhood of collinear libration center in restricted elliptical three-body problem, *Kosmicheskie Issledovaniia* 24 (4) (1986) 497–512.
- [10] A.Y. Kogan, An optimal program of impulse corrections of unstable periodic orbits, *Kosmicheskie Issledovaniia* 30 (5) (1992) 712–714.
- [11] C. Simó, G. Gómez, J. Llibre, R. Martínez, J. Rodríguez, On the optimal station keeping control of halo orbits, *Acta Astronaut.* 15 (6–7) (1987) 391–397.
- [12] G. Gómez, J. Llibre, R. Martínez, C. Simó, Station keeping of a quasiperiodic halo orbit using invariant manifolds, in: Proceed. 2nd Internat. Symp. on Spacecraft Flight Dynamics, Darmstadt, 1986, pp. 65–70.
- [13] T. Pavlak, K. Howell, Strategy for optimal, long-term stationkeeping of libration point orbits in the Earth-Moon system, in: AIAA/AAS Astrodynamics Specialist Conference Paper, AIAA 2012 - 4665.
- [14] D.C. Folta, T.A. Pavlak, A.F. Haapala, K.C. Howell, M.A. Woodard, Earth-Moon libration point orbit stationkeeping: theory, modeling, and operations, *Acta Astronaut.* 94 (1) (2014) 421–433.
- [15] D.J. Grebow, M.T. Ozimek, K.C. Howell, D.C. Folta, Multibody orbit architectures for lunar south pole coverage, *J. Spacecr. Rockets* 45 (2) (2008) 344–358.
- [16] K.C. Howell, H.J. Pernicka, Station-keeping method for libration point trajectories, *J. Guid. Control Dyn.* 16 (1) (1993) 151–159.
- [17] M. Ghorbani, N. Assadian, Optimal station-keeping near Earth-Moon collinear libration points using continuous and impulsive maneuvers, *Adv. Space Res.* 52 (12) (2013) 2067–2079.
- [18] K.C. Howell, T.M. Keeter, Station-keeping strategies for libration point orbits—Target point and Floquet Mode approaches, *Spacefl. Mech.* (1995) 1377–1396.
- [19] A.B. Molnar, Hybrid station-keeping controller design leveraging floquet mode and reinforcement learning approaches (Master's thesis), Purdue University, 2020.
- [20] V. Muralidharan, Orbit maintenance strategies for Sun-Earth/Moon libration point missions: Parameter selection for target point and Cauchy-Green tensor approaches (Master's thesis), Purdue University, 2017.
- [21] C.S. Subudhi, S. Vutukuri, R. Padhi, A near fuel-optimal station-keeping strategy for halo orbits, in: 2020 59th IEEE Conference on Decision and Control (CDC), IEEE, 2020, pp. 1478–1483.
- [22] C.M. Sakode, R. Padhi, Computationally efficient suboptimal control design for impulsive systems based on model predictive static programming, *IFAC Proc. Vol.* 47 (1) (2014) 41–46.
- [23] R. Padhi, M. Kothari, Model predictive static programming: a computationally efficient technique for suboptimal control design, *Int. J. Innovative Comput. Inf. Control* 5 (2) (2009) 399–411.
- [24] H.B. Oza, R. Padhi, Impact-angle-constrained suboptimal model predictive static programming guidance of air-to-ground missiles, *J. Guid. Control Dyn.* 35 (1) (2012) 153–164.
- [25] NASA JPL Horizons web-interface, 2021, <https://ssd.jpl.nasa.gov/horizons.cgi>. (Accessed 13 January 2021).
- [26] N. Assadian, S.H. Pourtakdoust, Multiobjective genetic optimization of Earth-Moon trajectories in the restricted four-body problem, *Adv. Space Res.* 45 (3) (2010) 398–409.
- [27] S. Vutukuri, Spacecraft trajectory design techniques using resonant orbits (Ph.D. thesis), Purdue University, 2018.
- [28] G. Gómez, Dynamics and Mission Design Near Libration Points: Fundamentals—the Case of Collinear Libration Points, vol. 1, World Scientific, 2001.
- [29] M.J. Turner, Rocket and Spacecraft Propulsion: Principles, Practice and New Developments, Springer Science & Business Media, 2008.
- [30] T.M. Lovelly, A.D. George, Comparative analysis of present and future space-grade processors with device metrics, *J. Aerosp. Inf. Syst.* 14 (3) (2017) 184–197.
- [31] A. Banerjee, R. Padhi, Multi-phase MPSP guidance for lunar soft landing, *Trans. Indian Natl. Acad. Eng.* (2020) 1–14.
- [32] K. Sachan, R. Padhi, Waypoint constrained multi-phase optimal guidance of spacecraft for soft lunar landing, *Unmanned Syst.* 7 (02) (2019) 83–104.
- [33] G. Gómez, K. Howell, J. Masdemont, C. Simó, Station-keeping strategies for translunar libration point orbits, *Adv. Astronaut. Sci.* 99 (2) (1998) 949–967.
- [34] A. Farrés, G. Gómez, J. Masdemont, C. Webster, D. Folta, The geometry of stationkeeping strategies around libration point orbits, in: 70th International Astronautical Congress, Washington DC, 1986.

